DESIGN OF THE LOW-SPEED NLF(1)-0414F AND THE HIGH-SPEED HSNLF(1)-0213 AIRFOILS WITH HIGH-LIFT SYSTEMS

J. K. Viken
Complere, Incorporated
Hampton, Virginia

S. A. Viken
Complere, Incorporated
Hampton, Virginia

W. Pfenninger
Analytical Services and Materials, Incorporated
Hampton, Virginia

H. L. Morgan, Jr. and R. L. Campbell
NASA Langley Research Center
Hampton, Virginia

OUTLINE

The Fluid Physics Branch (formerly Airfoil Aerodynamics Branch) at LaRC has been involved extensively in the design and testing of Natural Laminar-Flow (NLF) air-foils. The design of the NLF(1)-0414F was initiated in June of 1981 and completed in the summer of 1983 (ref. 1). This NLF airfoil was designed for low speed, having a low profile drag at high chord Reynolds numbers. When the wind tunnel experiment was completed in the spring of 1984 (ref. 2), a high lift system design for the NLF(1)-0414F was initiated.

The success of the low speed NLF airfoil work sparked interest in a high speed NLF airfoil applied to a single engine business jet with an unswept wing. Work began in the fall of 1984 on the two-dimensional airfoil design of HSNLF(1)-0213. The design of HSNLF(1)-0213 was conducted as a cooperative effort of several different groups at NASA LaRC with not only 2-D design but also extensive 3-D design and analy-sis of the wing's planform (ref. 3). Only the preliminary stages of the 2-D design will be discussed in the current paper (fig. 1). To make this single engine business jet successful, acceptable values of maximum lift had to be maintained to get the correct landing speed; therefore, work was also conducted on the 2-D flap design (ref. 4).

● Design of NLF(1)-0414F

● High lift system for NLF(1)-0414F

● Design of HSNLF(1)-0213

● High lift system for HSNLF(1)-0213

Figure 1

COMPARISON OF PRESSURE DISTRIBUTIONS OF NLF(1)-0414F
AND NACA 67-314

NLF(1)-0414F was designed iteratively using analysis computer codes. After going through the design study and obtaining experimental results, it is interesting to look at the comparison and contrast of NLF(1)-0414F with a similar NACA 6-series airfoil (fig. 2). NACA 67-314 was generated, using ref. 5, for the same incompressible C_ℓ, at $\alpha = 0$, and maximum thickness as NLF(1)-0414F ($M = 0.4$ and $C_\ell = 0.461$). The favorable gradient regions are similar, although NLF(1)-0414F has slightly more acceleration on each surface. The upper surface acceleration of NLF(1)-0414F was optimized by the use of the flat spot in the pressure distribution at $x/c \approx 0.10$. The Tollmien-Schlichting (TS) disturbances are not amplified in this region, so the stabilizing effects of acceleration can be used further downstream when the TS disturbances are amplified. Concave type pressure recoveries are utilized on NLF(1)-0414F, while on the NACA 67-314, linear pressure recoveries are used. NLF(1)-0414F has a thicker, tailored leading edge than NACA 67-314. Also, a small chord trailing-edge (cruise) flap was utilized on NLF(1)-0414F and is crucial to the low drag performance.

In the summary of airfoil data (ref. 6), there is only one NACA 67-series airfoil, the NACA 67,1-215. There are no data above $R = 6 \times 10^6$, presumable because the higher Reynolds number data produced little laminar flow. There are some differences between the old NACA experiments and those conducted on NLF(1)-0414F which could make a difference on the performance of the two airfoils. The NACA tests were run with 2-foot chord models, which were at higher unit Reynolds numbers for the same chord Reynolds number as the 3-foot chord NLF(1)-0414F. Also the grit used to cause transition in the NACA tests was considerably larger and more extensive than needed to cause transition.

COMPARISON OF PRESSURE DISTRIBUTIONS
OF NLF(1)-0414F & NACA 67-314
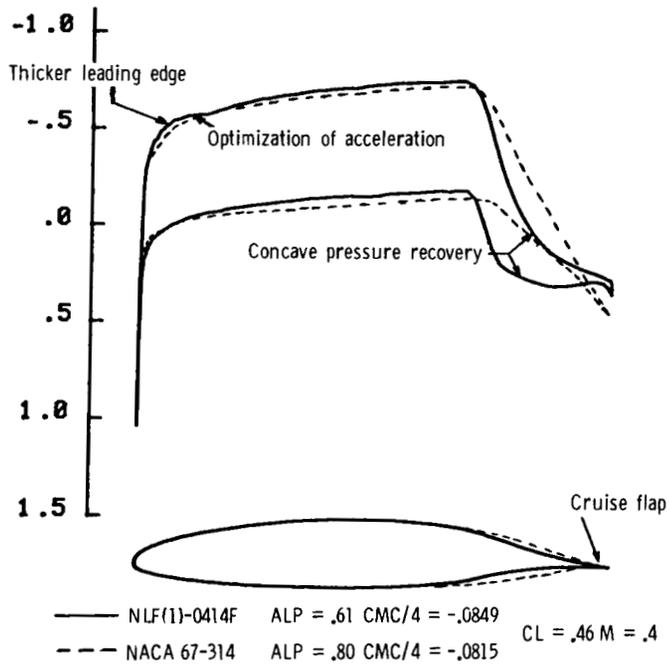
Figure 2

NLF(1)-0414F DESIGN OBJECTIVES

The first and primary objective of the design project was to design a Natural Laminar-Flow (NLF) airfoil, for low speed applications that achieved significantly lower profile drag coefficients at cruise than existing NLF airfoils, but was still practical to use (fig. 3). This resulted in an exercise to design an airfoil with as extensive favorable gradients (dp/dx < 0) as seemed practical without making the far aft pressure recoveries too severe. The airfoil was also designed for reasonably high chord Reynolds numbers, approximately 10 million.

To help lessen the severity of the far aft pressure recoveries with respect to separation, concave type pressure recoveries were utilized. A concave pressure recovery decelerates the flow when the boundary layer has the most energy, tapering the gradient of the deceleration downstream on the airfoil as the boundary loses energy. For off-design conditions, the possibility of utilizing boundary layer re-energizers or momentum redistributors was also examined as a means of alleviating the problem of turbulent separation in the pressure recovery.

To improve $C_{\ell_{max}}$ performance, a thicker leading edge was utilized than is normally considered for airfoils with such extensive laminar flow operating at such high chord Reynolds numbers. It was known that this thick leading edge would limit the low drag C_{ℓ} range on the bare airfoil with premature negative pressure peaks; however, the chance of a leading-edge type stall would be reduced. Also, Pfenninger's earlier work (ref. 7) showed that the use of a small chord simple trailing-edge flap could be used to regain a respectable low drag C_{ℓ} range. Deflection of this small chord flap, both positively and negatively, allows the conversion of lift due to angle of attack into lift due to flap deflection. By changing the lift at the design angle of attack, favorable gradients can be maintained on both surfaces simultaneously for a relatively wide range of lift coefficients.

When designing configurations for maximum cruise performance, one is inevitably led to flying as close to $(L/D)_{max}$ as possible. This means increasing the wing loading and results in the need for greater maximum lift coefficients. The NLF(1)-0414F was designed with the intent of integrating it with a slotted Fowler flap arrangement and possibly even a Krueger flap to achieve high maximim lift coefficients.

NLF (1)-0414F DESIGN OBJECTIVES

● 70% chord natural laminar flow (NLF) on both surfaces at Re_c = 10 million

● Compromise some low drag C_l range (at δ_f = 0°) to improve $C_{l_{max}}$ performance by thickening the leading edge

● Increase low drag C_l range with a small chord trailing edge flap

● Implement concave pressure recovery to reduce the turbulent separation problem when transition occurs far forward on the airfoil. Also, possibly use some form of boundary layer re-energization or momentum redistribution

● Use of boundary-layer trips (tape, grit, bleed air, etc.) to eliminate laminar separation at lower Reynolds numbers, both in the rear pressure recovery and at the leading edge at high angles of attack

● Implementation of an efficient high lift system: slotted Fowler flaps and possibly a Krueger flap

Figure 3

LAMINAR BOUNDARY-LAYER STABILITY ANALYSIS

The first stage in the design was to conduct a linear stability analysis in the favorable pressure gradient region to check for the attainability of the 70% chord laminar flow. On a high Reynolds number NLF airfoil, enough acceleration is needed to attain the desired growth in TS disturbances. This acceleration essentially requires a geometry increase along the chord. Unfortunately, this increase is not the only consideration. The leading edge needs to be thick enough for acceptable C_ℓ max performance; however, the maximum thickness cannot be too great because of pressure recovery considerations.

A linear stability analysis was conducted on the inviscid pressure distribution (ref. 8) for the upper surface of NLF(1)-0414F at the design conditions $M = 0.4$, $C_\ell = 0.461$ and $R = 10 \times 10^6$ (fig. 4). The velocity profiles were calculated using the Kaups and Cebeci finite-difference code (ref. 9) and the TS amplification was calculated using the SALLY code (ref. 10). The design criterion for NLF(1)-0414F for maximum logarithmic amplification (n) was in the range of 9 to 10. The analyzed disturbance frequencies of 3000-3500 Hz were in this maximum amplified range. The locally higher growths after 70% chord are from the increased instability at the beginning of the steep pressure recovery.

INCOMPRESSIBLE T S

T-S FREQ., Hz	n_{max}
○ 1000.	.557
□ 1500.	1.809
◇ 2000.	4.782
2500.	7.980
▲ 3000.	10.221
▲ 3500.	10.812
□ 3500.	10.812
● 5000.	7.669
● 6000.	6.098
● 7000.	4.826
● 8000.	3.949

<---> STABLE REGION

Pressure coefficient, C_p

Chord station, x/c   Chord = 4.00   J = 406.364

NLF1-0414F   M=.400   ALP= -.953   CL= .461   US   R = 10.0MIL
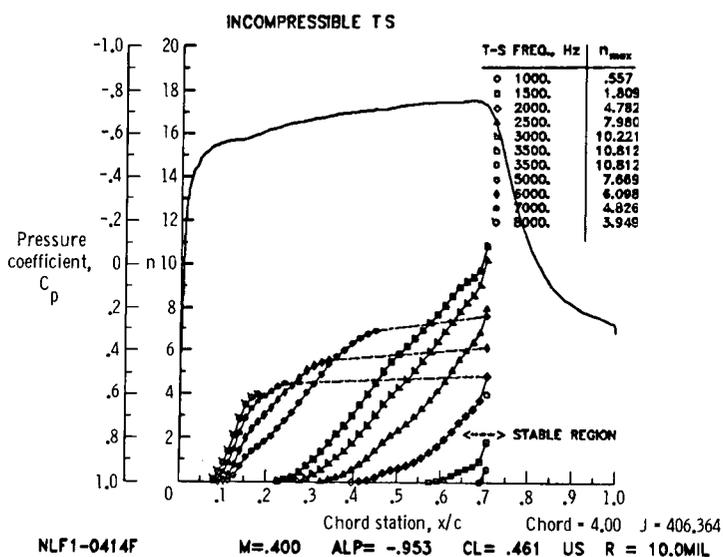
Figure 4

INCOMPRESSIBLE TS STABILITY ANALYSIS WITH UPPER SURFACE
MEASURED TRANSITION LOCATIONS

Shown in figure 5 are three cases analyzed for TS amplification up to transition on the experimental data of the NLF(1)-0414F in the Langley Low-Turbulence Pressure Tunnel. These cases were for the upper surface at C_ℓ's ranging from 0.409-0.513. Correlating linear stability theory with transition data, n factors in the range of 11-12 were calculated for the three cases at $M \approx .12$ and $R = 10 \times 10^6$.
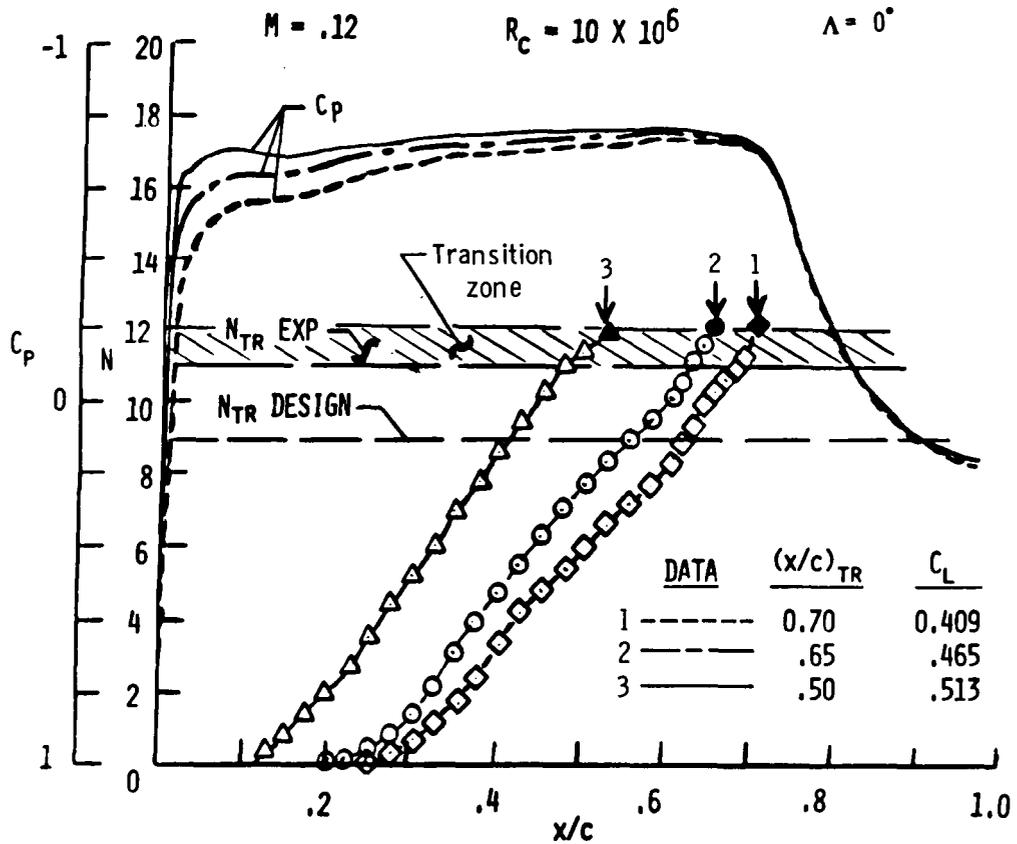
Figure 5

NLF(1)-0414F TURBULENT PRESSURE RECOVERY

The next step in the design process was to reduce the problem of turbulent separation in the pressure recovery when transition occurred near the leading edge. The energy deficient turbulent boundary layer has to have enough energy to negotiate a steep aft pressure recovery. The first route in designing the turbulent pressure recovery was to make it concave in nature, $\dfrac{d^2p}{dx^2} < 0$. This type of recovery decelerates the flow most at first when the boundary layer becomes more and more energy deficient. The pressure recovery was tailored using the growth in shape factor $H = \delta^*/\theta$. Schubauer and Spangenberg (ref. 11) found that for incompressible turbulent boundary layers the shape factor grows to a value of 2.0 at separation. Using the inviscid pressure distribution and the Harris finite-difference boundary layer code (ref. 12), the growth of H was tailored through the pressure recovery. To get a gradual progression of separation at off design conditions, H should grow continuously to a maximum value at the trailing edge. The H distribution in the pressure recovery for NLF(1)-0414F in figure 6 shows the shape factor growing to a maximum value of 1.9 at x/c = 0.875 with a slight decrease to 1.825 at the trailing edge. It was felt that this offered some margin for down cruise flap deflections and was left as is.

NLF1-0414F   M=.400   ALP= .610   CL= .461   US   R = 10.0MIL
FULLY TURBULENT
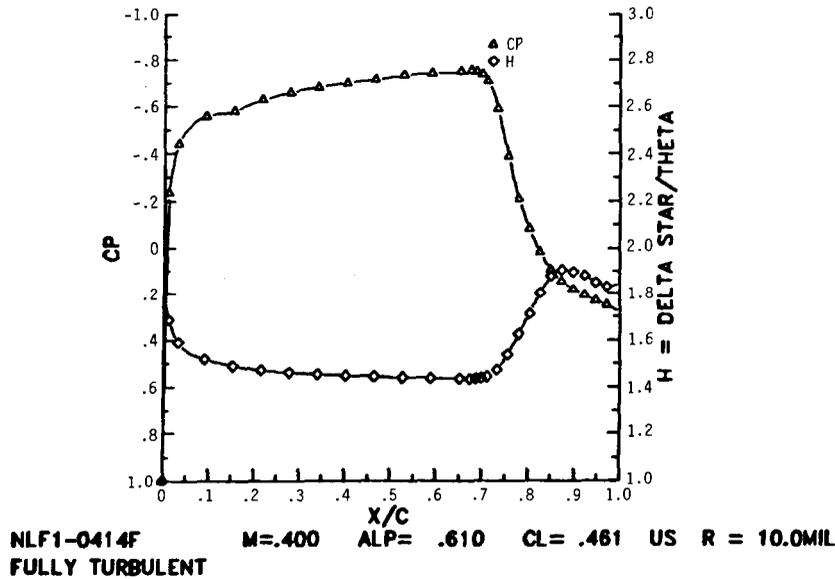
Figure 6

Figure 7 shows the turbulent boundary layer analysis on the upper surface inviscid pressure distribution of the NACA 67-314 airfoil. The points shown represent the results of the boundary-layer solutions, and because of separation, the pressure distribution does not continue to the trailing edge. For the same conditions as NLF(1)-0414F (M = 0.4, C_ℓ = 0.461, and R = 10 × 10^6), turbulent boundary-layer separation occurred at x/c = 0.90 in the linear pressure recovery. The last correct solution calculated H to be at a value of 1.83.
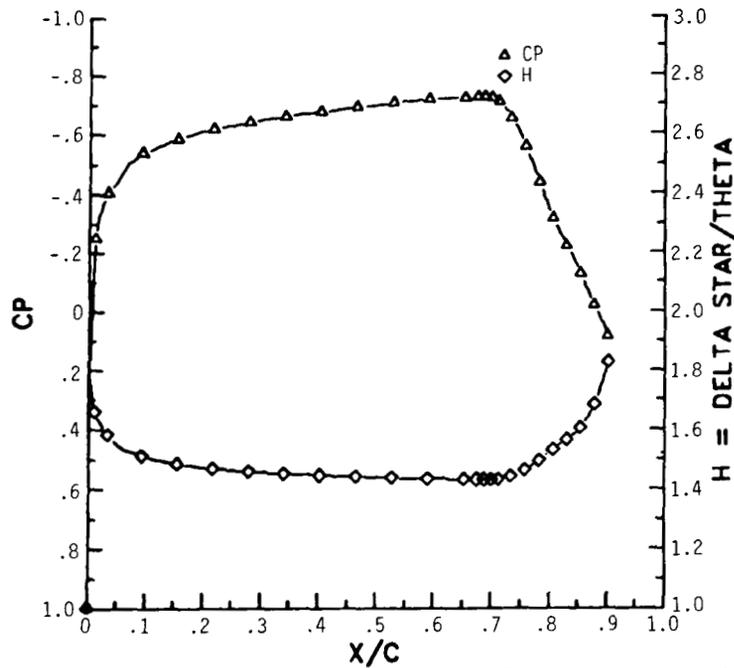
NACA 67-314   M=.400   ALP= .793   CL= .461   US   R = 10.0MIL
FULLY TURBULENT

Figure 7

COMPARISON OF AIRFOIL LEADING EDGES

Extensive work was conducted in the design of the leading edge of the NLF(1)-0414F. Early in the design process a sharp leading-edge airfoil, DESB159 (fig. 8), was implemented to achieve an acceptable low drag C_ℓ range at $\delta_f = 0°$. In the low drag range, this sharp leading edge helps suppress leading-edge negative pressure peaks. However, at high angles of attack this sharp leading edge causes large negative pressure peaks as a result of the centripetal forces $C_p \approx \frac{V^2}{R}$ needed to turn the air molecules around the corner. To obtain the leading edge of NLF(1)-0414F, thickness was superimposed on the airfoil profile merging with DESB159 at $x/c = 0.15-0.20$. Then the leading edge was tailored to reduce the negative pressure peaks. The design philosophy was to turn the flow when the velocity was low, allowing a smaller radius of curvature. The radius of curvature was then increased as the velocities grew. On both the DESB159 and NACA 67-314 profiles, the smallest radius of curvature is at the leading edge, where the smallest radius of curvature on the NLF(1)-0414F profile is on the lower surface.
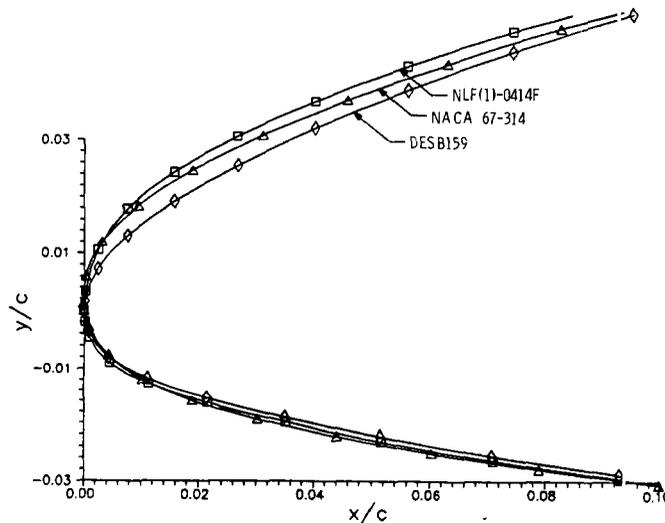
Figure 8

Figure 9, which is a plot of the inviscid $C_{P_{min}}$ as a function of C_{ℓ} shows how successful this tailoring of the leading edge was. At an inviscid C_{ℓ} of 1.8, NLF(1)-0414F had a $C_{P_{min}}$ of -8.5 as compared with a $C_{P_{min}}$ of -11.4 on DESB159. At an inviscid C_{ℓ} of 2.7, NLF(1)-0414F had a $C_{P_{min}}$ of -21.2 as compared with a $C_{P_{min}}$ of -30.3 for DESB159. The free-stream Mach number was 0.10.
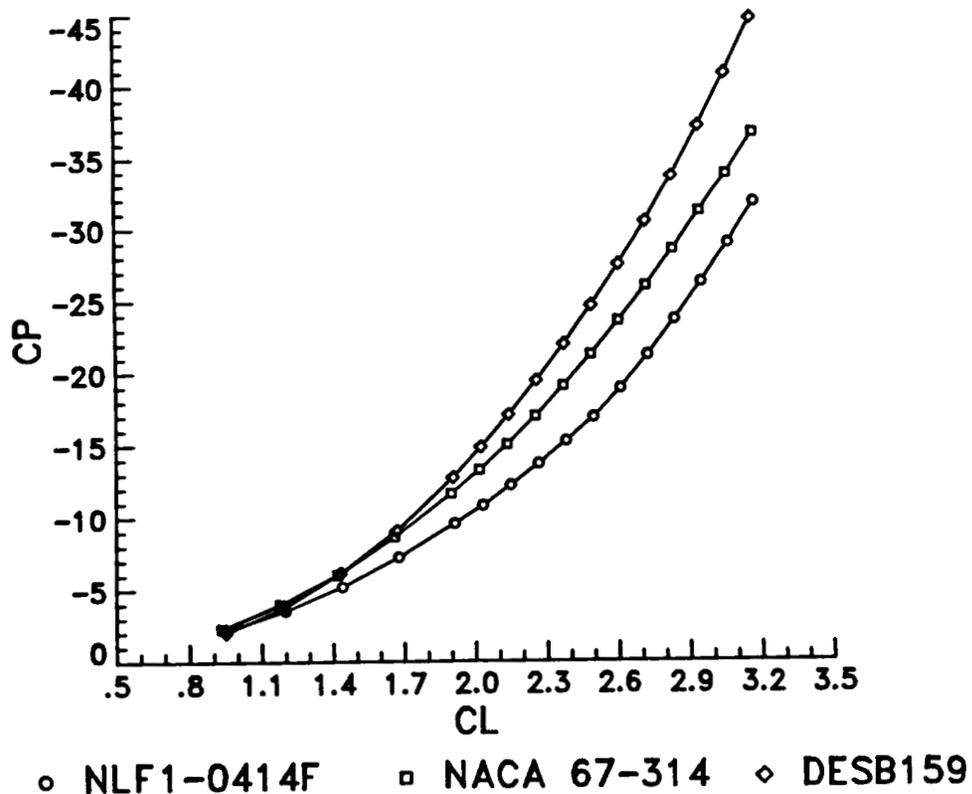
Figure 9

CRUISE FLAP DEFLECTION

Figure 10 illustrates the movement of the 12.5% chord cruise flap of NLF(1)-0414F deflection from -10° to 12.5°. The use of the cruise flap was crucial with the implementation of the thickened leading edge to achieve an acceptable C_ℓ range with low drag. The deflection of the cruise flap allows lift due to angle of attack to be converted into lift due to flap deflection by loading or unloading the aft section of the airfoil. With the use of this flap, different C_ℓ's can be achieved while still keeping the stagnation point near the leading edge and thereby keeping favorable gradients over the airfoil for a wide range of conditions.
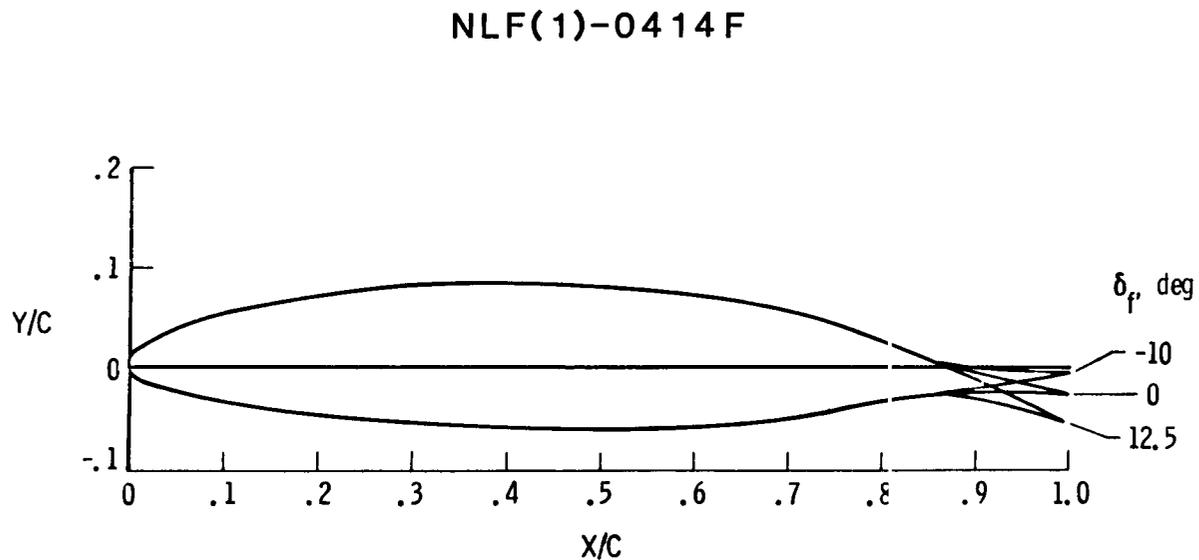
NLF(1)-0414F

Figure 10

The drag polar of NLF(1)-0414F (fig. 11), at $R = 10 \times 10^6$ for $\delta_f = -10°$ to 12.5°, reflects the success of achieving a wide low drag C_ℓ range with the use of the cruise flap. At $\delta_f = 0°$ there was a very narrow low drag C_ℓ range with the very bottom of the bucket having a $C_{d_{min}}$ of 0.0027 at $C_\ell = 0.41$. With a negative 10 degree flap deflection, the minimum drag was 0.0030 at $C_\ell = 0.01$. With a cruise flap deflection of 12.5°, the minimum profile drag was 0.0033 at a C_ℓ of 0.81 yielding a L/D of 245. The use of the cruise flap yields an overall low drag C_ℓ range of 0.80 at the high design chord Reynolds number of 10×10^6.

FLAP DEFLECTION EFFECTS
$M \leq 0.12 \quad R = 10.0 \times 10^6$
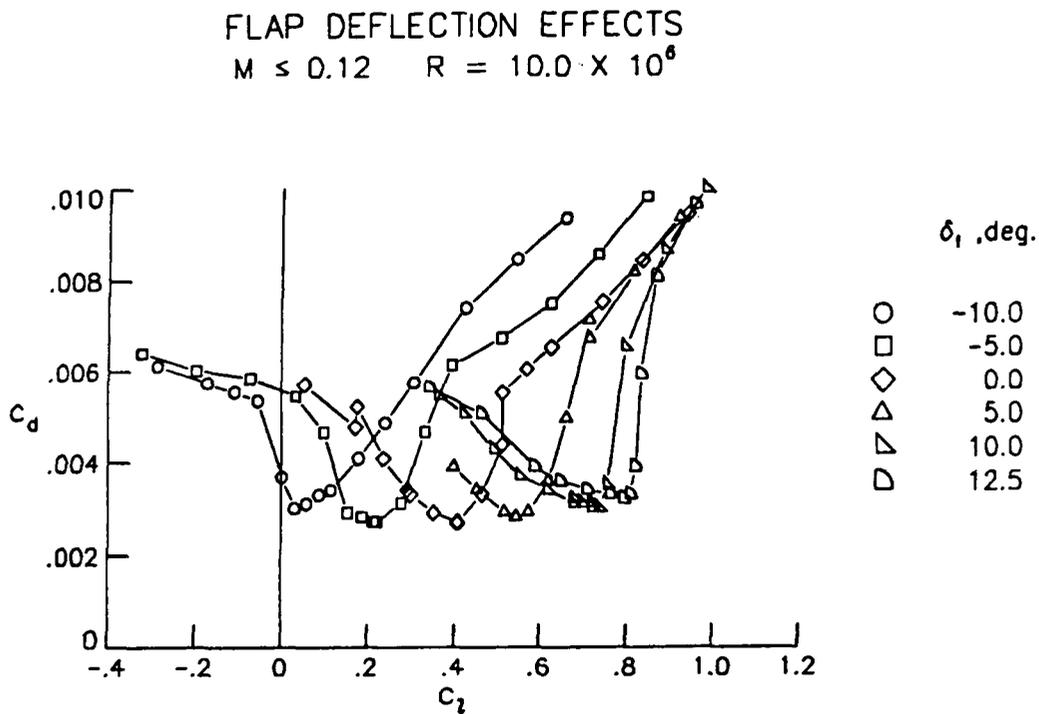
Figure 11

EXPERIMENTAL/THEORETICAL PRESSURE DATA AT DESIGN CONDITIONS

A comparison of the experimental pressure distribution of NLF(1)-0414F at
$M = 0.4$, $R = 10 \times 10^6$, and $\alpha = -1°$ is compared with the theoretical pressure
distribution calculated by the Korn-Garabedian potential flow analysis in fig-
ure 12. There are favorable gradients on both surfaces up to the 70% chord loca-
tion. The steep concave pressure recoveries of NLF(1)-0414F are also illustrated.
There is a flat spot in the upper surface pressure distribution at $x/c = 0.15$. This
resulted from the addition of thickness in the leading-edge region to improve $C_{\ell_{max}}$
performance. Results from the Tollmien-Schlichting boundary-layer stability analysis
showed that this flat spot in the pressure distribution yielded a smaller disturbance
growth than with a continuous acceleration in this region.
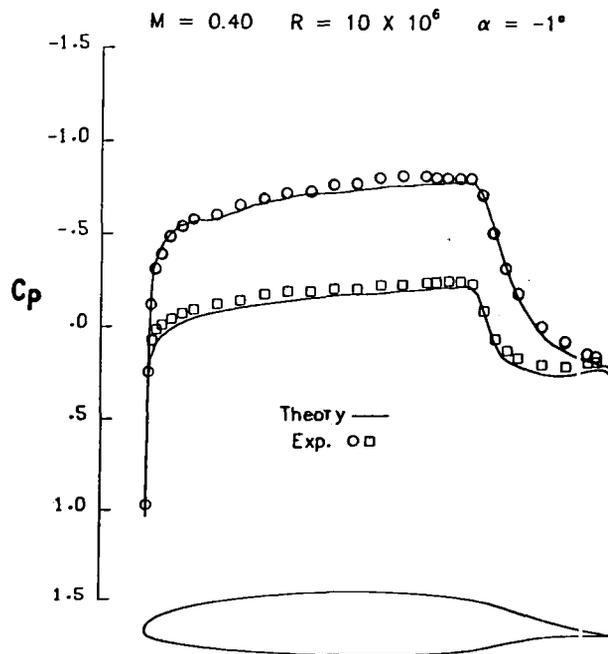
Figure 12

The section characteristics of NLF(1)-0414F at a chord Reynolds number of
10 million and $\delta_f = 0°$ are shown in figure 13. The minimum profile drag coef-
ficient was 0.0027 at $C_\ell = 0.41$. This profile drag is only 38% that of an unsepa-
rated fully turbulent airfoil. The maximum lift coefficient is 1.83 at $\alpha = 18.0°$.
With transition fixed at the leading edge the lift curve essentially repeated with
$C_{\ell_{max}}$ still 1.81. The pitching moment curve is unaffected with fixed transition.
With the flow fully turbulent, the minimum profile drag coefficient is 0.0083, which
is equal to that of normal unseparated turbulent airfoils.
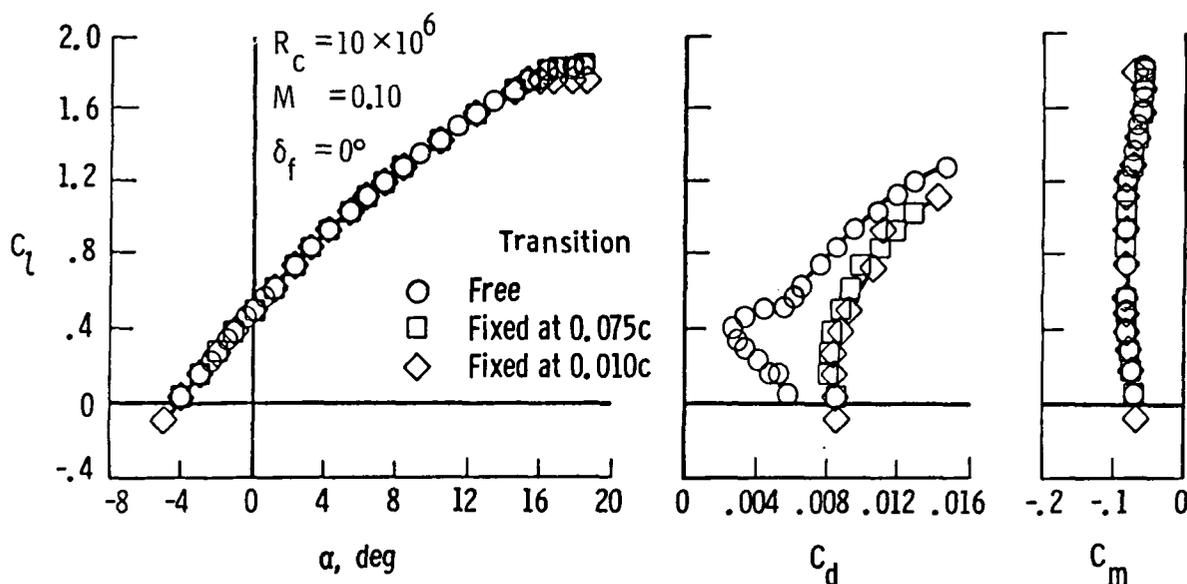
Figure 13

COMPARISON OF GA AIRFOILS

Figure 14 is a comparison of the low drag bucket of NLF(1)-0414F with other NASA and NACA general aviation (GA) airfoils at $R = 6 \times 10^6$. The low drag bucket of NLF(1)-0414F represents the envelope of low drag buckets achieved with deflection of the cruise flap from $-10°$ to $20°$. Also, the NLF(1)-0215F airfoil's low drag bucket is the envelope of performance of the deflection of a cruise flap from $-10°$ to $10°$. This figure shows the much lower profile drag coefficients possible with the NLF(1)-0414F. The large increase in profile drag of the NLF(1)-0414F outside the low drag bucket at the higher C_ℓ's is a result of the steep aft pressure recoveries.
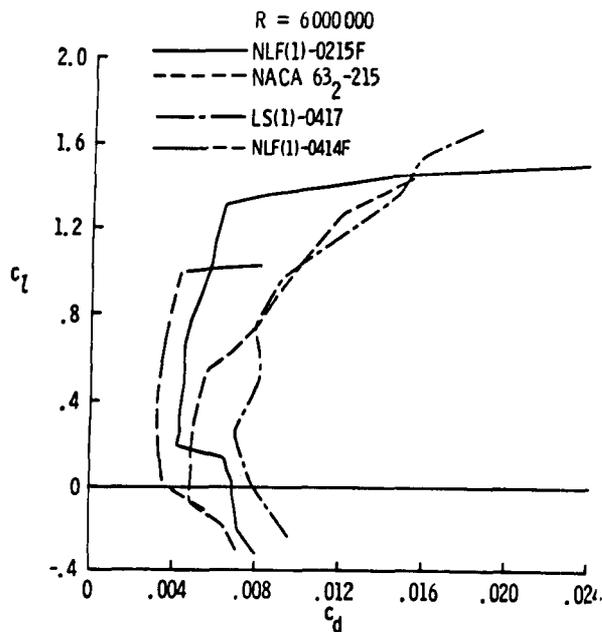
Figure 14

A multi-element high-lift flap system has been theoretically designed for the NLF(1)-0414F airfoil at a chord Reynolds number of 3 million and a free-stream Mach number of 0.15. The geometry consists of a main element, single-slotted Fowler flap or double-slotted Fowler flap (which retracts to form the single-slotted flap contour), and a Krueger flap. Both the leading- and trailing-edge high-lift systems have been integrated in a manner that still retains the action of a small chord trailing-edge cruise flap and implements as much as possible the original exterior profile contour of the NLF airfoil (fig. 15).

The main element has a chord of 0.896 with respect to the NLF airfoil chord of 1.0. The NLF contour is maintained over the entire extent of the upper surface, while on the lower surface, 70 percent of the contour is maintained before the cove region. Therefore, the 70 percent chord laminar-flow run on the upper and lower surface obtainable in the cruise condition is not disturbed.

The 28.1 percent chord single-slotted Fowler flap incorporates 10 percent of the airfoil's upper surface and 24 percent of the lower surface. The flap was designed not to exceed 30 percent of the airfoil's chord when it was retracted because the gap or step might cause transition.

The double-slotted Fowler flap was designed under the constraint that it would have the same outer contour as the single-slotted flap when retracted. The vane has a 15.81 percent chord, while the rear flap has a 16.52 percent chord (both based on the airfoil chord of 1.0).

The 17.67 percent chord Krueger flap (based on the NLF(1)-0414F chord of 1.0) was designed so that when retracted into the main element, 49.3 percent of the Krueger flap's upper surface would fare into the leading-edge lower surface of the NLF(1)-0414F. With a carefully designed sealed joint the flow should not be tripped turbulent.
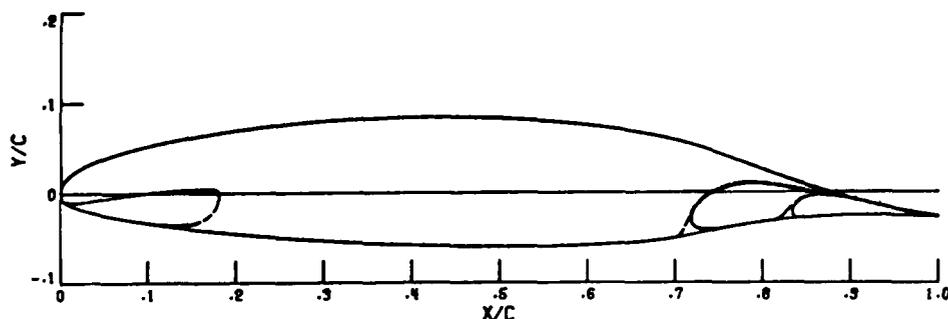
Figure 15

NLF(1)-0414F WITH SINGLE-SLOTTED FOWLER FLAP

The high lift performance for the two element system (main element and single-slotted Fowler flap) was analyzed using the potential flow multi-element analysis (MCARF ref. 13) code at $M = 0.15$, $\alpha = 7°$, and $\delta_f = 29°$, with an inviscid $C_\ell = 3.570$ and $C_{m_{c/4}} = -0.6082$ (fig. 16). The flap has a gap/c = 0.011 and overlap/c = 0.033 (relative to the main axis system). The total pressure rises calculated on the main element and flap upper surface were 88.05 percent q_{max} and 84.90 percent q_{max}, respectively. The Harris code was used to calculate the boundary-layer development on the MCARF inviscid pressure distributions at a chord Reynolds number of 3 million, with transition set slightly ahead of the $C_{P_{min}}$. The flow was calculated to stay attached to the trailing edge on the upper surface of the main element and separate at x/c = 0.704 on the lower surface (the beginning of the cove region). On the upper surface of the flap, 36.67 percent flap chord separation was calculated with a pressure rise of 66.53 percent q_{max}.

SINGLE-SLOTTED FOWLER FLAP PRESSURE DISTRIBUTION

Figure 16

The high lift performance for the multi-element system [Krueger flap, main element (10° flipper flap deflection), and double-slotted Fowler flap] at M = .15, α = 21°, δ_k = -55.4°, δ_{VF} = 34.4°, and δ_{RF} = 45.7°, with an inviscid C_ℓ = 6.627 and $C_{mc/4}$ = -0.4055 is shown in figure 17. The Krueger flap has a gap/c = 0.10 and overlap/c = 0.005, the vane has a gap/c = 0.018 and overlap/c = 0.033, and the rear flap has a gap/c = 0.014 and overlap/c = 0.008 (relative to the main axis system). The total pressure rises calculated on the Krueger flap, main element, vane, and rear flap upper surface were 81.67 percent q_{max}, 82.44 percent q_{max}, 84.77 percent q_{max}, and 84.90 percent q_{max}, respectively. The Harris code was used to calculate the boundary-layer development on the MCARF inviscid pressure distributions at a chord Reynolds number of 3 million, with transition set slightly ahead of the $C_{p_{min}}$. On the Krueger flap upper surface, 11.61 percent flap chord separation was calculated with a pressure rise of 63.38 percent q_{max}. For the main element upper surface, 5.91 percent main chord separation was calculated with a pressure rise of 79.35 percent q_{max}. The flow was calculated to separate at x/c = 0.708 on the main element lower surface. On the upper surface of the vane, 28.98 percent vane chord separation was calculated with a pressure rise of 40.10 percent q_{max}. The flow on the lower surface of the vane was calculated to separate in the cove region at x/c = 0.944. For the rear flap upper surface, 34.64 percent flap chord separation was calculated with a pressure rise of 63.24 percent q_{max}.

DOUBLE-SLOTTED FOWLER & KRUEGER FLAP PRESSURE DISTRIBUTION
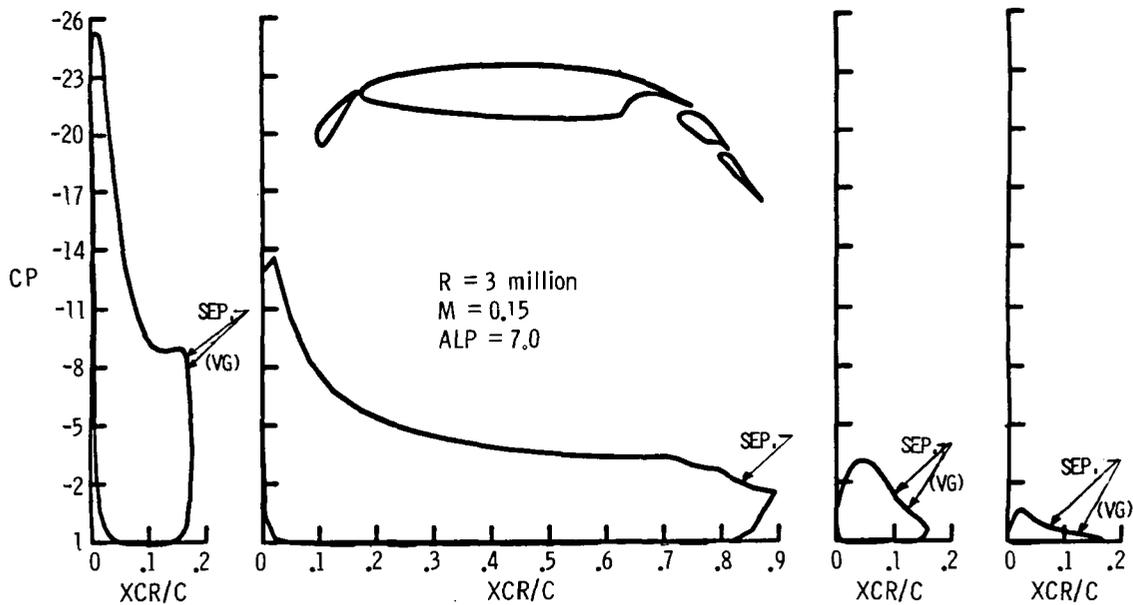
Figure 17

MAXIMUM LIFT POSSIBILITIES WITH NLF(1)-0414F MULTI-ELEMENT HIGH-LIFT SYSTEM

The NLF(1)-0414F airfoil can obtain a $C_{\ell_{max}}$ of 1.624 at a chord Reynolds number of 3 million. Estimations using inviscid pressure distributions at $R = 3 \times 10^6$ and finite-difference boundary layer calculations indicate very respectable maximum lift coefficients possible. For the cases analyzed, leading-edge negative pressure peaks were kept above C_p sonic (velocity below sonic), with overall inviscid pressure rises of 80-85% q_{max}. An analysis was also made to check for a leading-edge type stall using Horton's method (ref. 14). The results of these calculations indicated that leading-edge laminar separation bubbles would be short in nature, and the boundary layer would reattach for all cases. The multi-element high-lift system configurations designed from the NLF airfoil contour are shown in figure 18 which compare their relative performance with the baseline airfoil. The C_ℓ's are calculated from inviscid pressure distributions that were iterated with an integral boundary layer. No account has been made for separation.

The large negative C_p peaks and the corresponding steep adverse gradients caused during high angles of attack with large deflections bring about a separation problem. The flap placement, as well as the geometry, have distinct effects on the airfoil system as a whole. The effects help the turbulent boundary layer overcome a greater overall pressure rise than it would on a profile with the same outer contour without a slot. The flap must be placed such that the circulation of the main element reduces its leading-edge negative pressure peak at high angles of attack. Also, the flap's circulation should interact upon the main element to reduce the overall pressure rise by increasing the velocity field near the trailing edge. A leading-edge device will reduce the negative pressure peak on the leading-edge region of the following element, and hence the total pressure rise of that element overall.

HIGH LIFT SYSTEM FOR NLF1-0414F

(Chord Reynolds number of 3.0 million)
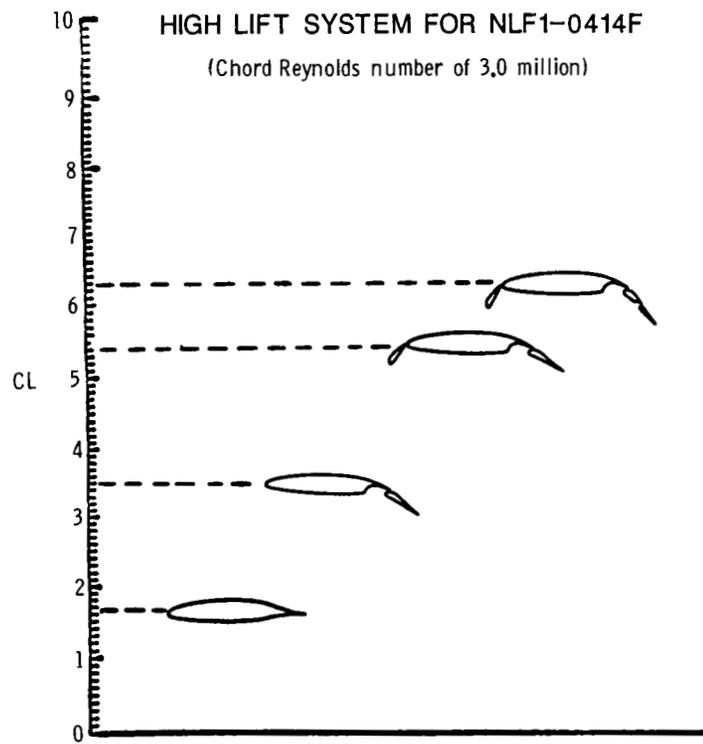
Figure 18

LOW-SPEED AIRFOIL SUMMARY

Figure 19 summarizes the results of the work on the 2-D profile, of the NLF(1)-0414F. Extensive work was conducted to make a high chord Reynolds number airfoil with low profile drag, while still making it practical to use. The NLF(1)-0414F at $R = 10 \times 10^6$ achieved a minimum profile drag coefficient of 0.0027 at $C_\ell = 0.41$. There was only a penalty in profile drag when transition occurred near the leading edge. The NLF(1)-0414F achieved a very respectable $C_{\ell_{max}}$ of 1.83. At worst, the NLF(1)-0414F is as good as a high Reynolds number turbulent flow airfoil except in the range of $C_\ell \approx 0.80$–1.2. The profile drags in this range are high because at these conditions the boundary layer can no longer make the turbulent pressure recovery. An experiment needs to be conducted on the high-lift system to verify the design and complete the basic work of making the NLF(1)-0414F a complete airfoil.

● Validated design theory for low-speed NLF(1)-0414F airfoil concept

● Achieved 70% chord NLF on both surfaces at design M = 0.4, $R_C = 10 \times 10^6$ in LTPT; total drag reduced 66% compared with turbulent airfoil

● Achieved wide low drag C_l range (C_l = 0 to 0.81) at high R_C with deflected 0.125C simple flap; L/D = 245 at C_l = 0.81

● Achieved $C_{l\,max}$ higher than expected; 1.83 with $\delta_f = 0°$ and 2.7 with 0.20C split flap ($\delta_f = 60°$). Achieved docile stall conditions

● Demonstrated that performance ($C_{l\,max}$ and pitch) essentially unchanged with fixed transition near leading edge with drag penalty compared to good turbulent airfoil

● Correlated linear boundary layer stability theory for design N-factor TS disturbances

● Multi-element high-lift system designed with a possibility of $C_{l\,max}$ > 6.0 for the Krueger flap, main element, and double-slotted flap configuration

Figure 19

The HSNLF(1)-0213 was an airfoil designed for $M_\infty = 0.70$, $C_\ell = 0.25$, and $R = 11 \times 10^6$ for application to a single-engine business jet with no sweep. The design considerations for a compressible airfoil design (fig. 20) are modified somewhat from that of the incompressible case. In compressible flow the laminar boundary layer is much more stable than in the incompressible case, so not as much acceleration is needed. Also as lift increases, overall acceleration increases instead of negative pressure peaks forming at the leading edge. This gives a wider low drag C_ℓ range. However, with this added acceleration, the recovery region becomes more of a problem when transition occurs far forward. Acceleration in the favorable gradients can quickly develop into shocks at higher than design C_ℓ's and Mach numbers.

COMPRESSIBLE AIRFOIL DESIGN
(NO SWEEP)

● Laminar boundary layer more stable in compressible flow than in the incompressible case - not as much accceleration needed

● Acceleration is not lost on upper surfaces as lift increases

● Turbulent pressure recovery more critical because flow accelerates to higher velocities than in incompressible case

● Watch for shock development in the acceleration

Figure 20

HSNLF(1)-0213 DESIGN PROCESS

As seen in figure 21, the camber and thickness of NLF(1)-0414F cause too much acceleration on the upper surface. The design of the high-speed airfoil had to be conducted rather hastily, so the easiest way to take out camber was to unload the airfoil by a negative deflection of the cruise flap. The resultant pressure distribution is shown in figure 22 at $M_\infty = 0.70$ with the 12.5% chord simple flap deflected -5.24°. This de-cambering was successful in reducing the upper surface velocities and the extent of the supersonic region, but there still was a steep aft pressure recovery. At a chord Reynolds number of 11 million with fully turbulent flow, analysis with the Harris program predicted separation in the aft pressure recovery for all of a series of possible recoveries. The next step in the design process was to redesign the upper surface, moving the start of the pressure recovery to $x/c = 0.55$ and flattening the pressure recovery. In the process, the overall thickness of the airfoil was reduced from 14% chord to 13% chord. The resultant airfoil is shown by the dotted line in figure 22.

EFFECT OF MACH NUMBER ON PRESSURE DISTRIBUTION OF NLF(1)-1414F
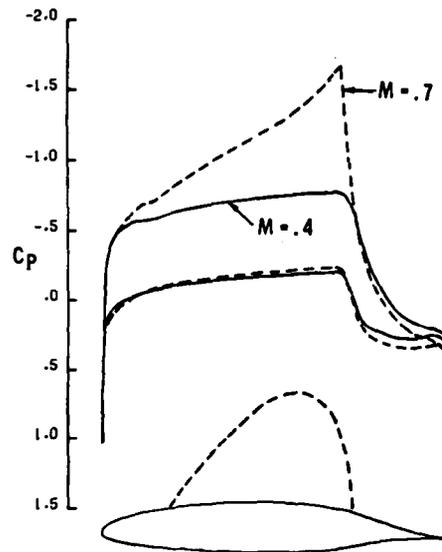
Figure 21

EFFECT OF MACH NUMBER ON PRESSURE DISTRIBUTION
OF NLF(1)-0414F

Some of the problems of using a low speed airfoil at high speed Mach numbers are illustrated in figure 21. The pressure distributions of NLF(1)-0414F are shown at M = 0.4 and M = 0.7. The M = 0.7 case accelerates strongly to the 70% chord location and terminates in a shock with a very steep aft pressure recovery. The supersonic zone is shown by the dotted line on top of the profile geometry. Note the negligible change in lower surface pressure coefficients between the two Mach numbers.

HSNLF(1)-0213 AIRFOIL DESIGN PRESSURE DISTRIBUTION

(M = .7)

Upper surface aft-thickness reduced

NLF(1)-0414F with neg. flap deflection

C_p
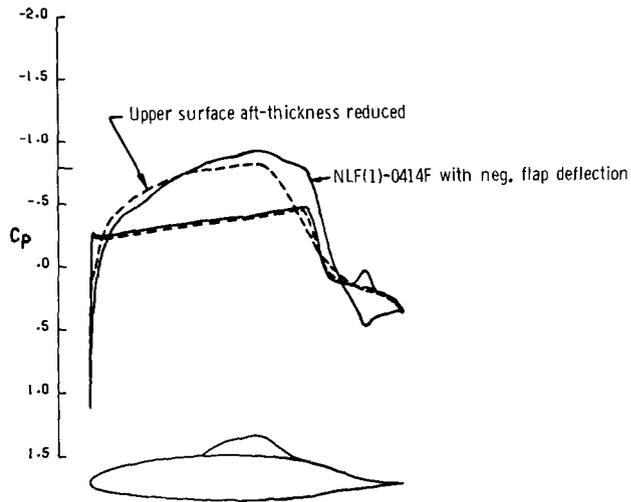
Figure 22

Figure 23 represents the pressure distribution at $M = 0.70$, $C_\ell = 0.25$, and $R = 11 \times 10^6$, for the final contour of HSNLF(1)-0213 compared to the NLF(1)-0414F airfoil with a -5.24° cruise flap deflection. The small leading-edge negative pressure peak was smoothed out from that shown in figure 22 in order to achieve the final contour of the HSNLF(1)-0213 airfoil.

$$M = 0.70 \quad C_\ell = 0.25 \quad R = 11 \times 10^6$$

FINAL AIRFOIL DEFINED WITH VIKEN DESIGNED UPPER SURFACE AND CAMPBELL DESIGNED LOWER SURFACE LEADING EDGE
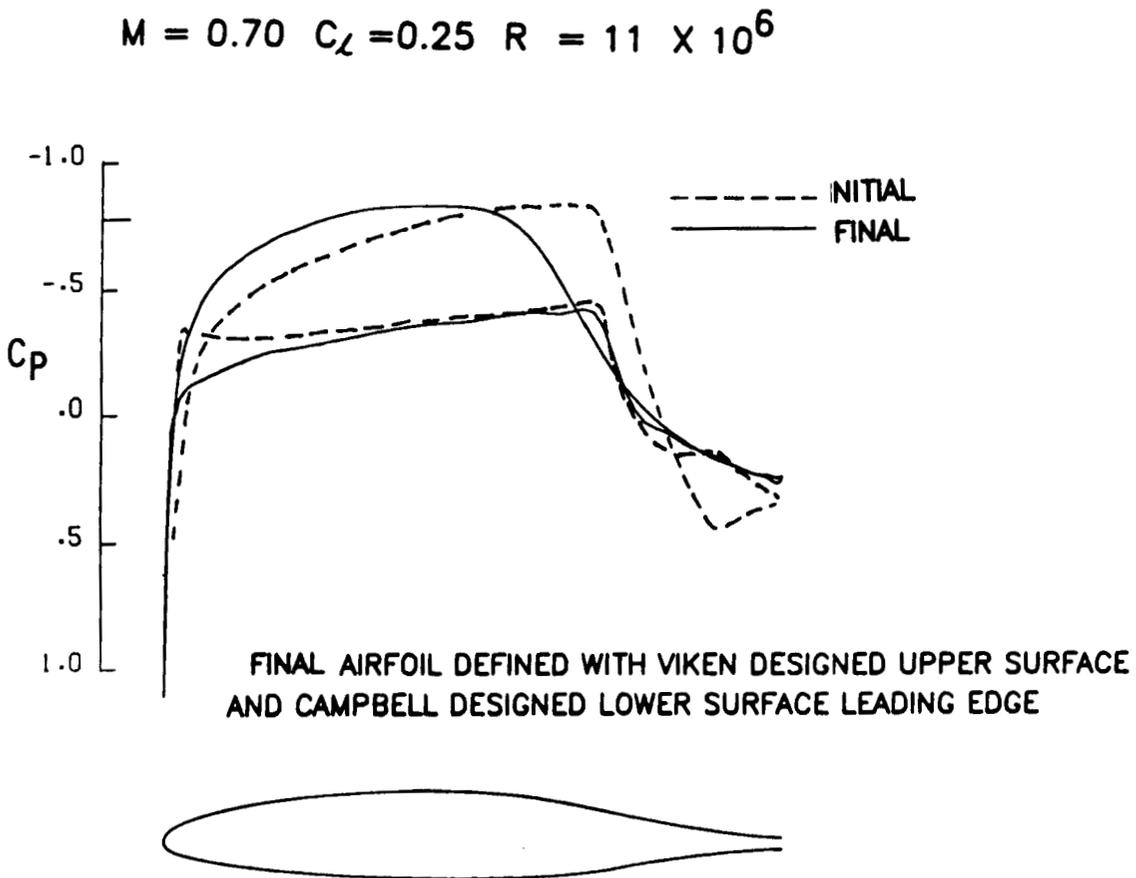
Figure 23

COMPRESSIBLE STABILITY ANALYSIS FOR HSNLF(1)-0213

The results of the compressible Tollmien-Schlichting analysis (ref. 15) for the upper surface of the HSNLF(1)-0213 at $M = 0.7$, $C_\ell = 0.26$, and $R = 10 \times 10^6$ are shown in figure 24. For the range of frequencies analyzed, the disturbances do not even start to grow until $x/c = 0.37$, and the maximum logarithmic amplification back to the laminar separation point is $n = 1.69$. This growth in TS disturbances is very small compared to the value of approximately $n = 9$ needed for transition. Therefore, TS disturbances should not cause transition in the accelerated region. This airfoil was designed for unswept applications. With sweep, care must be taken that cross-flow disturbances do not cause transition in the strong accelerated regions of the airfoil.

COMPRESSIBLE TS

T-S FREQ., Hz	n_{max}
o 2000.	0.000
□ 3000.	.468
◇ 4000.	1.111
▲ 4250.	1.308
◣ 4500.	1.551
◗ 4750.	1.633
◓ 5000.	1.688
◇ 6000.	1.353
◊ 7000.	.511
◠ 8000.	0.000

<---> STABLE REGION

PRESSURE COEFFICIENT, C_p

CHORD STATION, x/c

HSNLF1-0213   M=.700   ALP= -.953   CL= .260   US   R = 10.0MIL
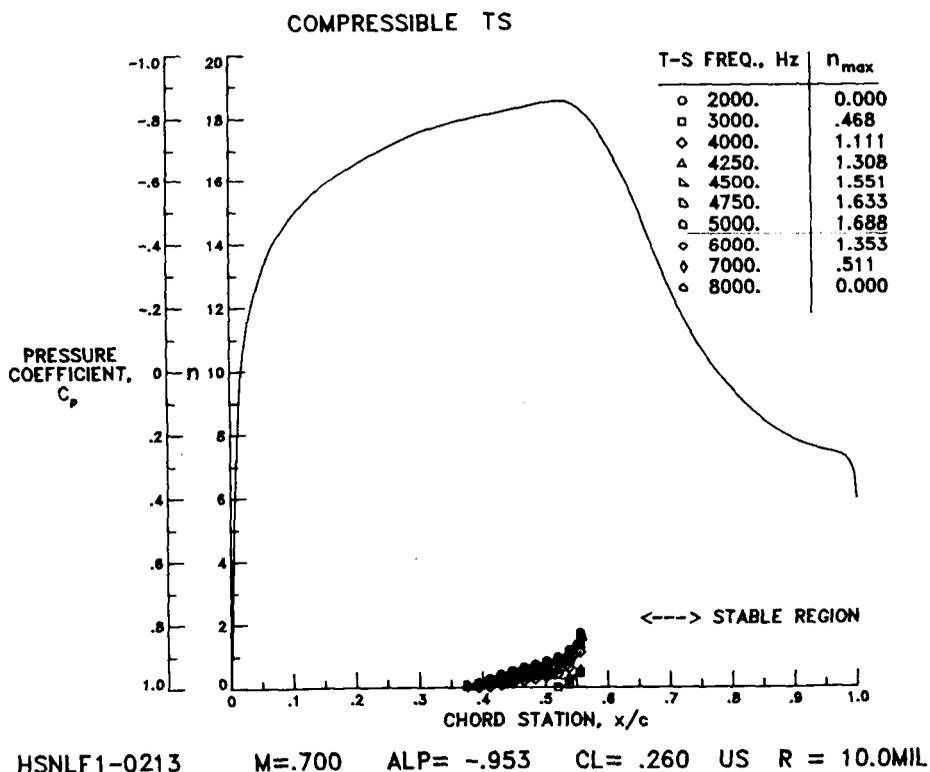
Figure 24

SINGLE-SLOTTED FLAP DESIGNS FOR HSNLF(1)-0213 AIRFOIL

The length of the structural wing box for most high speed general-aviation and transport aircraft is nominally 50 percent of the local wing chord and is positioned with 20 percent of the chord forward of the wing box available for leading-edge devices and 30 percent aft available for trailing-edge devices. For the HSNLF(1)-0213, an additional 2 percent immediately aft of the wing box was allowed for structural interface with a flap actuation system resulting in a nested trailing-edge flap chord length of 28 percent of the total wing chord. After establishing the basic chord length of the flap, the design of the flap contour became a matter of determining the upper and lower surface cutoff points on the main element and then determining the coordinates of the flap forward of the cutoff points. The cutoff point on the lower surface was set at 74 percent chord on the main element which was as far aft as possible to insure a smooth pressure recovery through the slot region between the flap and main elements. The selection of the upper surface cutoff point was not as simple. It was desirable to move the cutoff point as far as possible to increase the effective chord with the flap extended which should produce greater maximum lift. The primary disadvantage to moving the cutoff point aft is that the maximum thickness and leading-edge camber of the flap must be reduced to obtain an acceptable structural thickness in the trailing edge of the main element. The reduction in thickness and camber will most likely result in a reduction in maximum obtainable lift. During this design study upper-surface cutoff points at 88, 92, 96, and 98 percent of the main element chord were analyzed to determine the maximum obtainable lift. The flap geometries corresponding to the four cutoff points are presented in figure 25.
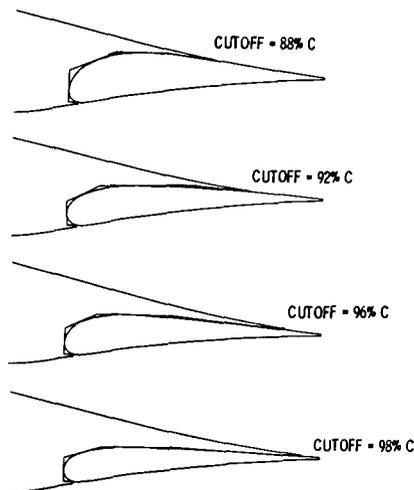
Figure 25

COMPARISON OF GEOMETRIES AND PRESSURE DISTRIBUTIONS
FOR SINGLE-SLOTTED HSNLF(1)-0213 FLAP DESIGNS

The performance of each of the four flap designs with various cutoff locations on the main element was determined using the NASA Multi-Component Airfoil Analysis (MCARF) computer program. The flap designs were analyzed for flap deflections of 35 and 40 degrees with a 2-percent gap and 0-percent overlap between the flap and main elements. The Mach number was 0.1 and the Reynolds number was 4 million. For each case, a check for flap separation was also made by performing an ordinary turbulent boundary-layer analysis of the upper-surface flap pressure distribution. As shown in figure 26, the turbulent boundary-layer analysis of the flap pressure distributions of each flap design at 35 degrees deflection indicated that approximately 31, 21, and 17 percent of the upper surface of the flap was separated for the 88-, 96-, and 98-percent designs compared to 14 percent for the 92-percent design. The comparison of the geometries also shown in this figure shows that the 92-percent design is proportionally thicker aft of the maximum thickness point compared to the others which reduced the upper surface pressure recovery resulting in less separation and higher maximum lift.

$(\delta_f = 35^0, R = 4 \times 10^6)$
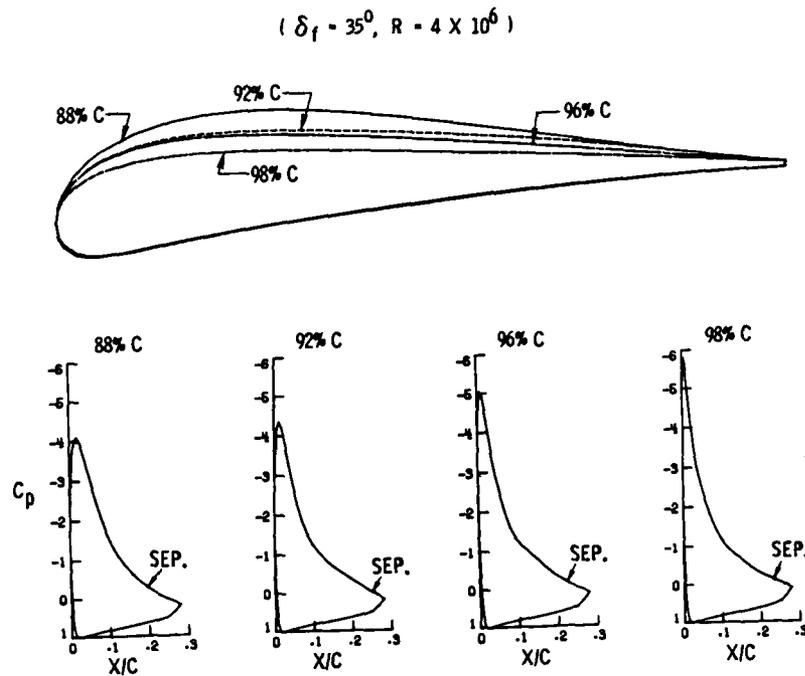
Figure 26

COMPARISON OF GEOMETRIES FOR SINGLE- AND DOUBLE-SLOTTED
FLAPS FOR HSNLF(1)-0213 AIRFOIL

A double-slotted trailing-edge flap was also designed for the HSNLF(1)-0213 airfoil to provide an additional increment of lift. The vane, which is the forward flap element, had to be concealed in the cove region, and the aft-flap element had the same design constraints as that for the single-slotted flap design. The vane-flap combination was designed so that the vane remained in a fixed position relative to the aft-flap when deflected. A simple fixed external-hinge mechanism was proposed as the flap actuation device. A comparison of the finalized single- and double-slotted flap geometries is presented in figure 27. The vane element has a chord of 8 percent and the aft-flap a chord of 20.5 percent of the wing chord. The upper surface cutoff point on the main element was moved from 92 to 87 percent for the double-slotted design to allow for the passage of the vane element through the cove opening for flap deflections greater than 20 degrees. For flap deflections greater than 25 degrees, the lower surface trailing-edge deflector can be deflected upward into the cove approximately 15 degrees to improve the acceleration of the flow through the slot. The primary advantage of the double-slotted design is that the second slot allows for additional energization of the flap boundary layer which will further delay separation and increase the maximum obtainable lift.

DOUBLE- AND SINGLE-SLOTTED FLAPS FOR HSNLF(1)-0213 AIRFOIL

(a) DOUBLE-SLOTTED FLAP

(b) SINGLE-SLOTTED FLAP
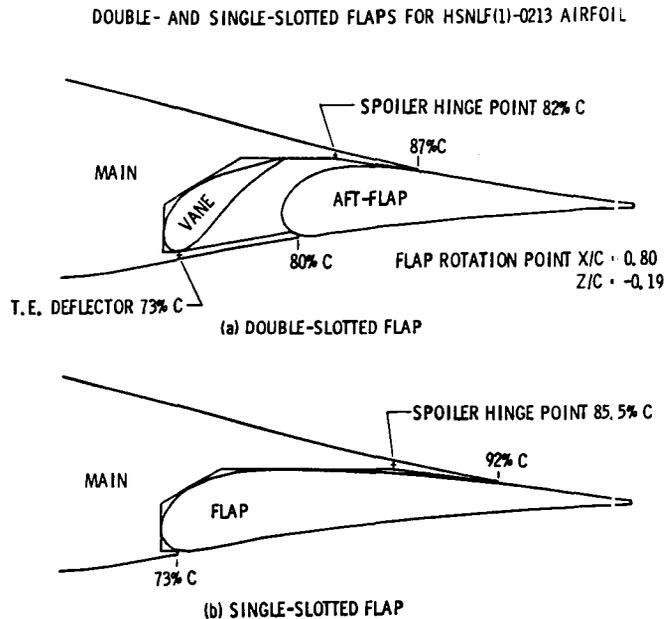
Figure 27

MAXIMUM LIFT PERFORMANCE OF HSNLF(1)-0213 WITH SINGLE- AND DOUBLE-SLOTTED FLAPS

The effect of Reynolds number on the maximum lift performance of the double-slotted flap at 55 degrees of deflection and the single-slotted flap at 40 degrees of deflection is presented in figure 28. The maximum lift values shown are based on separation of the leading-edge laminar boundary layer on the main element and do not include corrections for the effect of trailing-edge separation on the flap elements. These data show the tremendous effect of Reynolds number on the maximum lift obtainable for both types of flaps, especially at Reynolds numbers below 4 million. This trend is typical for Natural Laminar-Flow (NLF) airfoils that have small leading-edge radii which produce highly favorable pressure gradients at low angles of attack for large runs of laminar flow on both surfaces. At higher angles of attack near stall these small leading-edge radii produce rather highly unfavorable pressure gradients that are very sensitive to separation.

EFFECT OF REYNOLDS NUMBER
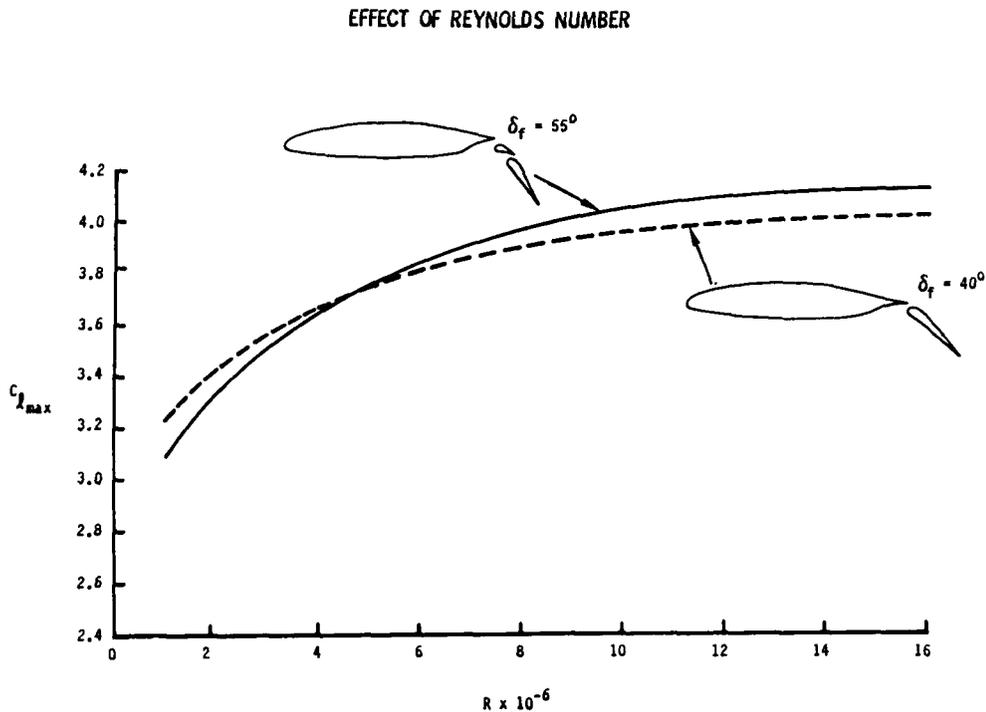
Figure 28

Figure 29 summarizes the work done on the 2-D airfoil design of the HSNLF(1)-0213. The airfoil was decambered by removing the aft loading; however, higher design Mach numbers are possible by increasing the aft loading and reducing the camber overall on the airfoil. This approach would also allow for flatter acceleration regions which are more stabilizing for cross-flow disturbances. Sweep could then be used to increase the design Mach number to a higher value also. There would be some degradation of high lift by decambering the airfoil overall, and this aspect would have to be considered in the final design.

SUMMARY

● Shock-free NLF airfoil designed for M = 0.70 and C_l = 0.26 for applications without sweep

● High-speed airfoil designed with favorable gradients back to 55% chord on upper surface and 65% chord on lower surface

● Linear stability analysis in the laminar boundary layer indicated that at the design point compressible Tollmien-Schlichting disturbances were not large enough to cause transition before laminar separation

● Upper surface turbulent pressure recovery optimized so that no separation occurred at design when transition occurred at the leading edge

● Single-slotted and double-slotted Fowler flap designs were optimized to get acceptable low-speed characteristics

Figure 29

REFERENCES

1. Viken, Jeffrey K.: Aerodynamic Considerations and Theoretical Results for a High Reynolds Number NLF Airfoil. Master's Thesis, George Washington University, January 1983.

2. McGhee, Robert J.; Viken, Jeffrey K.; Pfenninger, Werner; Beasley, William D.; and Harvey, William D.: Experimental Results for a Flapped NLF Airfoil with High Lift/Drag Ratio. NASA TM-85788, May 1984.

3. Waggoner, Edgar G.; Campbell, Richard L.; Phillips, Pamela S.; and Viken, Jeffrey K.: "Computational Design of Natural Laminar Flow Wings for Transonic Application", Langley Symposium on Aerodynamics, Volume I, NASA CP-2397, pp. 415-444. April 1985.

4. Morgan, Harry L.: "High Lift Flaps for Natural Laminar Flow Airfoils", Laminar Flow Aircraft Certification, NASA CP-2413, April 1985, pp. 31-66.

5. Ladson, Charles L., and Brooks, Cuyler W., Jr.: Development of a Computer Program to Obtain Ordinates for NACA 6- and 6A-Series Airfoils. NASA TM X-3069, Sept. 1974.

6. Abbott, Ira H., and von Doenhoff, Albert E.: Theory of Wing Sections: New York: Dover Publications Inc., 1959.

7. Pfenninger, W.: Investigations on Reductions of Friction on Wings, in Particular by Means of Boundary Layer Suction. NACA Technical Memorandum 1181, August 1947.

8. Bauer, F., Garabedian, P., and Korn, D.: A Theory of Supercritical Wing Sections, with Computer Programs and Examples. New York: Springer-Verlag, 1972.

9. Kaups, Kalle, and Cebeci, Tuncer: User's Guide for a Computer Program to Calculate Compressible Laminar Boundary Layers With Suction on Swept and Tapered Wings. Douglas Aircraft Co.

10. Srokowski, Andrew J.; and Orszag, Steven A.: Mass Flow Requirements for LFC Wing Design. AIAA Paper No. 77-1222.

11. Schubauer, G. B., and Spangenberg, W. G.: Forced Mixing in Boundary Layers. National Bureau of Standards Report No. 6107, August 1958.

12. Harris, Julius E., and Blanchard, Doris K.: Computer Program for Solving Laminar, Transitional, or Turbulent Compressible Boundary-Layer Equations for Two-Dimensional and Axisymmetric Flow. NASA Technical Memorandum 83207, February 1982.

13. Stevens, W. A.; Goradia, S. H.; and Braden, J. A.: Mathematical Model for Two-Dimensional Multi-Component Airfoils in Viscous Flow. NASA CR-1843, June 1971.

14. Horton, H. P.: A Semi-Empirical Theory for the Growth and Bursting of Laminar Separation Bubbles. Aeronautical Research Council Current Paper No. 1073, June 1967.

15. Malik, Mujeeb R.: COSAL—A Black Box Compressible Stability Analysis Code for Transition Prediction in Three-Dimensional Boundary Layers. NASA CR-165925, May 1982.